J Mater Sci: Mater Electron
DOI 10.1007/s10854-012-0693-x

Growth of CdS nanoparticles in Y- and Z-type Langmuir–Blodgett thin film using 1,3-bis-(*p*-iminobenzoic acid) indane

T. Uzunoglu · H. Sari · R. Capan · H. Namli · O. Turhan · G. A. Stanciu

Received: 13 December 2011 / Accepted: 12 March 2012

Abstract Cadmium sulphide (CdS) nanoparticles were formed in 1,3-bis-(*p*-iminobenzoic acid)indane by exposing Cd^{2+} doped Y- and Z-type multilayered Langmuir–Blodgett (LB) films to H_2S gas. The growth of CdS nanoparticles were monitored by UV–visible spectroscopy measurements. It was observed that CdS nanoparticles in both Y- and Z-type LB films cause a blue-shift in absorption spectra. The surface morphology of LB films were characterized with atomic force microscopy DC electrical measurements were carried out for these LB films grown in a metal/LB film/metal sandwich structures with and without CdS nanoparticles. By analyzing I–V curves and assuming Schottky conduction mechanism the barrier height was found to be as 1.25 and 1.17 eV for Y-type unexposed and exposed samples; 1.18 and 1.25 eV for Z-type unexposed and exposed samples, respectively.

T. Uzunoglu (✉) · R. Capan (✉)
Department of Physics, Faculty of Arts and Science, Balıkesir University, Çağış, 10145 Balıkesir, Turkey
e-mail: tuzunoglu@balikesir.edu.tr

R. Capan
e-mail: rcapan@balikesir.edu.tr

H. Sari
Department of Engineering Physics, Faculty of Engineering, Ankara University, Tandoğan, 06100 Ankara, Turkey

H. Namli · O. Turhan
Department of Chemistry, Faculty of Arts and Science, Balıkesir University, Çağış, 10145 Balıkesir, Turkey

G. A. Stanciu
Department of Physics, Center for Microscopy, Microanalysis and Information Processing, University "Politehnica" of Bucharest, Bucharest, Romania

1 Introduction

II–VI semiconductor nanoparticles, such as cadmium sulphide (CdS) [1] and zinc sulphide (ZnS) [2–4] within organic multilayer thin film grown by Langmuir–Blodgett (LB) deposition technique have been studied recently. The size, shape and distribution of semiconductor nanocluster in organic LB films are better controlled using LB film technique. In this technique the size of the nanoparticles mainly depends on the organic molecules [4] as well as the growing procedure [5].

CdS have direct bulk phase band gap of 2.4 eV at room temperature, therefore it is one of the most important II–VI semiconductor used in light emitting optoelectronic devices such as LEDs [6]. By shrinking size, such semiconductors show quantum effect which allows fabrication of very efficient electronic and optoelectronic devices. Therefore, a great deal of effort has been put recently on both growth and characterization of such nanoparticles in LB films [7]. The observation of the blue shift of absorption bands is major development for the fabrication of light emitting devices [8]. Conductive polymers mixed with semiconducting nanoparticles (CdS, CdSe, CuS, or ZnS) show new properties [9].

It is also well known that group II (cadmium and zinc) ions interact with carboxylic acid head groups (COO^-) and thus the ions can easily accommodate in a multilayer LB film structure [10, 11]. When such multilayer assemblies were exposed to H_2S gas, the group II ions reacted with sulphide ions to produce corresponding II–VI nanoparticles expressed with this reaction $(C_{23}H_{16}N_2O_4)_2[X]^{2+} + H_2S \rightarrow 2[C_{23}H_{16}N_2O_4H] + XS$ [11, 12]. Here X is the group II atoms (Zn or Cd).

In this work, we report the growth details of both Y- and Z-type 1,3-bis-(*p*-iminobenzoic acid)indane (IBI) multilayer LB films containing CdS semiconducting nanoparticles and

Published online: 03 April 2012

the effect of these nanoparticles on electrical properties by means of UV–visible absorption spectroscopy, atomic force microscopy (AFM), and electrical measurements.

2 Experimental details

The chemical structure of 1,3-bis-(*p*-iminobenzoic acid)indane molecule (IBI) is shown in Fig. 1. While the IBI molecule has two hydrophilic carboxylic acid sites and conjugation through all the double bonds it could be expected that the molecule can hold the Cd^{2+} ions better than that of molecule which has only one carboxylic head. The hydrophobic aromatic rings and carbonyl group double bonds are in conjugation, thus the electrical and chemical properties of the LB film expected to have different properties than that of classical amphiphilic molecules.

To prepare solution for the film growth IBI molecules were dissolved in a 9:1 ratio of chloroform and methanol solvent mixture. Using a NIMA 622 type alternate layer LB trough, the cadmium chloride was dissolved in the subphase as reach to 0.5 mg/ml concentration of solution because it is well known that cadmium ions interact with carboxylic acid head group and thus cadmium ion can be easily accommodated in a multilayer LB film structure [11]. IBI solution was spread onto the water surface and a time period of 15 min was allowed for the solvent to evaporate before the area enclosed by the barriers was reduced. The π–A isotherm graph of IBI with and without Cd^{2+} ions was recorded as a function of surface area using the compression speed of 25 mm/min. Isotherm graph given in Fig. 2 was repeated several times and the results were found to be reproducible.

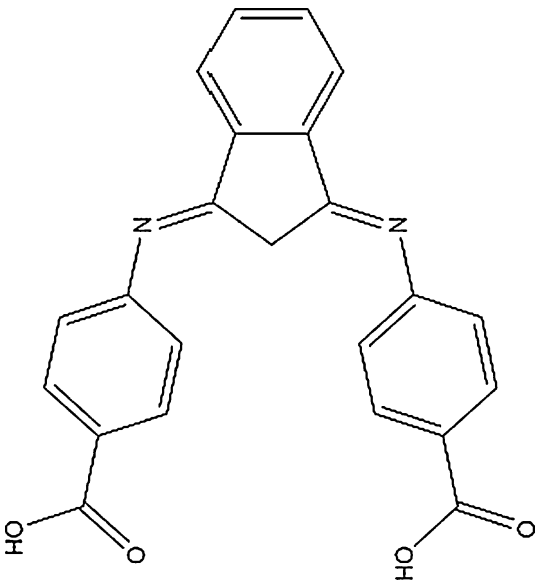

Fig. 1 Chemical structure of 1,3-bis-(*p*-iminobenzoic acid)indane (IBI)

Cadmium ions interact with carboxylic head group of IBI organic molecules. Therefore, the difference of isotherms was observed due to the effects of metal ions [13], which is consisted with the reported data of Ppy with Cu^{2+} ions, which have slightly smaller areas than that of Ppy without Cu^{2+} ions [14]. We know that the difference of isotherms with/without Cd^{2+} ions could result in the difference in electrical properties [15, 16]. Using the isotherm graph, the deposition pressure of 20 mN/m was selected to produce both Y- and Z-type LB films in the thickness of 15 monolayer for optical measurements. The solution was spread onto the water surface using a microlitre syringe and approximately 15 min were allowed for the chloroform to evaporate before the area enclosed by the barriers was reduced. Monolayer at the water surface were sequentially transferred onto quartz substrates by the alternate layer LB deposition procedure. The monolayer of IBI was transferred with a speed of 10 mm/min. The temperature of the water subphase was controlled using Lauda Ecoline RE 204 model temperature control unit and all experimental data were taken at room temperature. Optical measurements were taken by ocean optics UV–visible light source (DH-2000-BAL deuterium tungsten light source) and spectrometer (USB4000) in absorbance mode. The wavelength was changed from 300 to 850 nm by covering the ultraviolet and visible spectral region. Different layer numbers were chosen for AFM and electrical measurements. AFM measurements were performed using a Quesant 350 scanning probe microscope. The scale is set in such a way that light colors correspond to higher structures. The AFM images were taken using a standard silicon nitride tip (constant force 12 N/m) in the contact mode. The surface morphology change of LB films before and after H_2S gas exposure was monitored using AFM images. For electrical measurements HP 4192A impedance analyzer, Keithley 228A current source, Keithley 6514

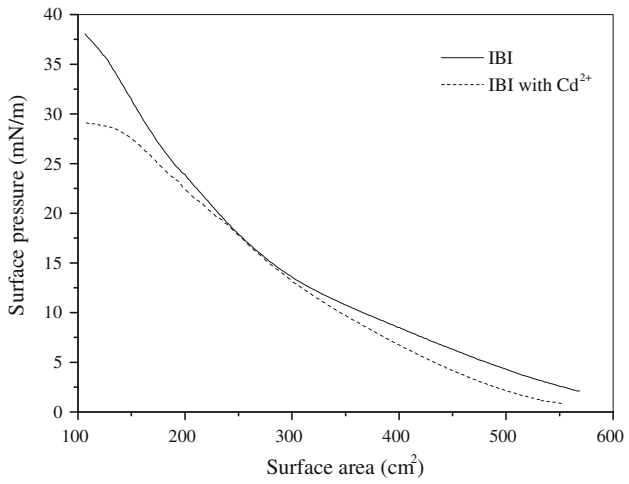

Fig. 2 Isotherm graph of 1,3-bis-(*p*-iminobenzoic acid)indane (IBI) with and without cadmium ions

voltmeter, and Keithley 485 ampermeter were used. All the data was collected automatically by using GPIB interface card and labview data acquisition software.

In order to check the effect of CdS nanoparticles within the LB films the previously prepared samples were cut into two pieces. One of them was exposed to hydrogen sulphide gas (H_2S) for 45 min and the other half was used as reference purpose. For the electrical measurements, the LB film grown on Al-coated substrate was placed into a thermal evaporator for top electrode fabrication right after the exposure of H_2S gas. Top electrodes were fabricated under 8×10^{-7} mbar vacuum by evaporating aluminium using a mask which has 16 parallel, 1 mm $\times$ 15 mm sized opening grids on it. Special care is given not to damage the organic films during the evaporation, such as using the possible lowest evaporation rate 3 Å/s. The final structure of metal/LB films/metal configuration and carboxylic head groups of molecules incorporation with Cd^{2+} in Z- and Y-type LB films are shown in Fig. 3a. Figure 3b show that CdS nanoparticles in Z- and Y-type films were occurred after the films were exposed H_2S gas.

3 Results and discussion

3.1 UV–visible results

Figure 4 shows UV–visible absorption spectra of the 15 and 20 monolayer thick Y- and Z-type LB films taken before and after H_2S gas exposure. After the exposure of

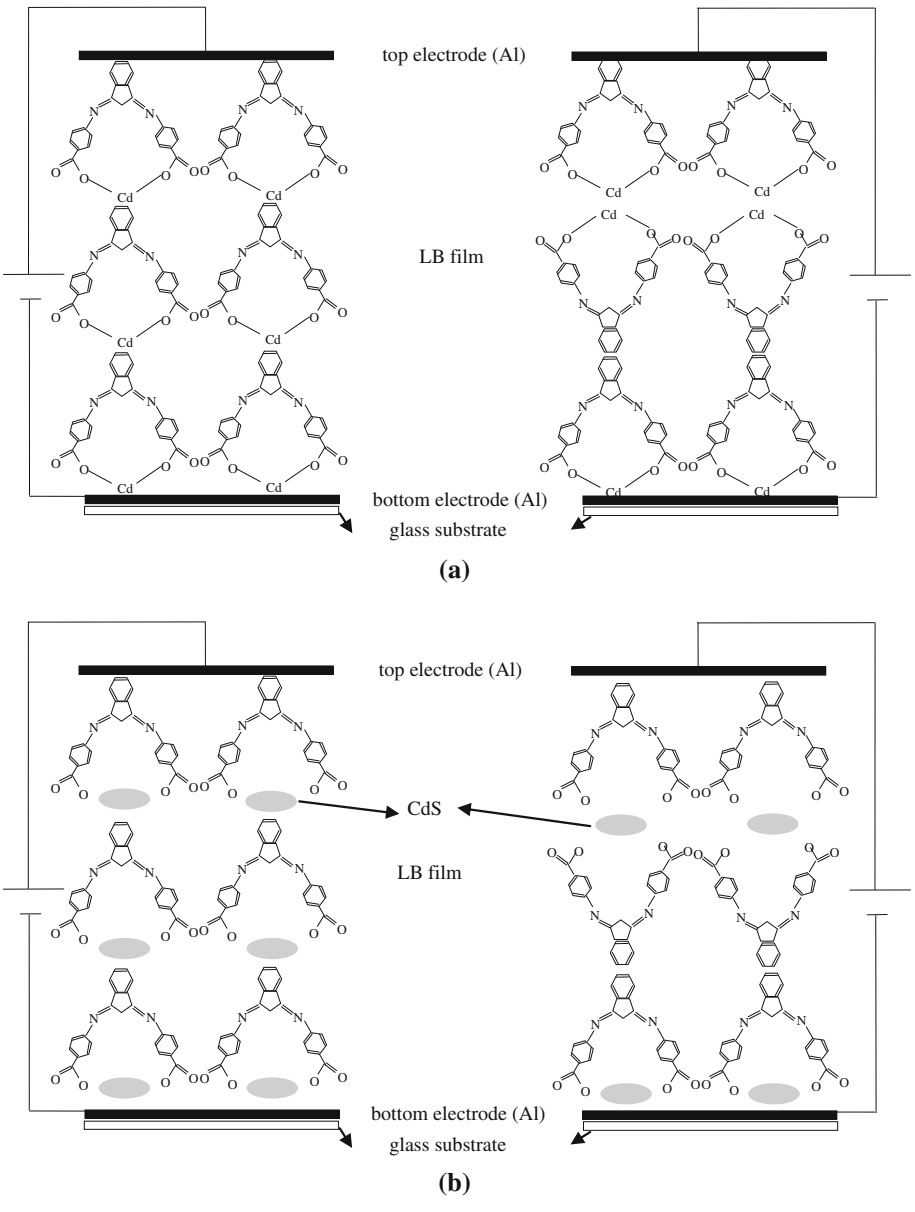

Fig. 3 The device structure of LB film for electrical measurements **a** Z- and Y-type before H_2S gas, **b** Z- and Y-type after H_2S gas

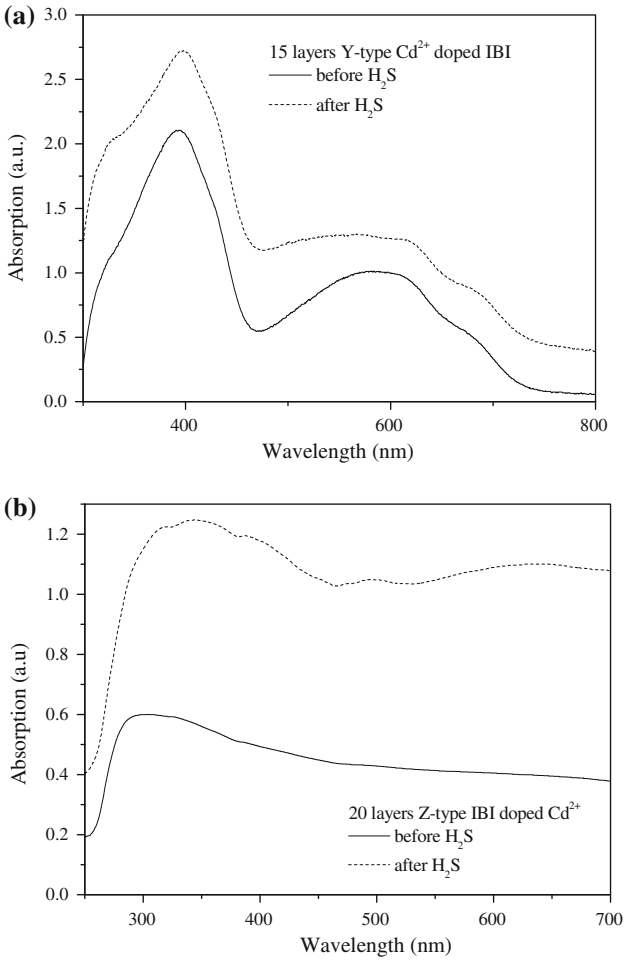

Fig. 4 UV absorption spectra for **a** Y-types 15 multilayer LB films and **b** Z-types 20 multilayer LB films, before (*solid*) and after (*dashed*) exposure to H_2S gas

H_2S gas to the LB films, some changes at the UV–vis spectra occurred due to the formation of CdS nanoparticles in the LB multilayers [2]. When absorption spectra curves are compared an additional absorption peak appears on the absorption onset of the exposed sample. We have studied ZnS nanoparticles previously and found similar changes [3]. The absorption peak seen at 323 nm on the onset of the absorption spectra of the Y-type LB film is due to exitonic absoption band of CdS. The blue shift relative to the bulk CdS ($\lambda_g^{bulk} = 512$ nm) is 189 nm. The shift has occurred due to formation of CdS nanoparticles. For the Z-type LB film containing CdS nanoparticles it is at around 315 nm, which is 197 nm blue-shifted relative to the bulk CdS ($\lambda_g^{bulk} = 512$ nm) [2]. The existence and the shifts of the peaks resulting from by exposing the films to H_2S gas support the formation of the nanoparticles and their nanoparticles nature [17]. The shift is the result of the size quantization and its magnitude is proportional to the size of the nanoparticles (R) according to the equation [18–20]:

$$E_{(0,1)} = E_g + \frac{\left(\frac{\hbar}{2\pi}\right)^2 \phi_{(0,1)}^2}{2\mu R^2} \quad (1)$$

where $E_{(0,1)}$ is energy quantum levels for electrons and holes in the conduction and valance bands, $E_g = 2.425$ eV is the energy gap of bulk CdS, $m_e^* = 0.153$ is the effective mass of electrons, $m_h^* = 0.7$ is effective mass of holes [12], $\phi_{(0,1)} = \pi$ series of Bessel function roots, and μ is the reduced mass given by:

$$\frac{1}{\mu} = \frac{1}{m_e^*} + \frac{1}{m_h^*} \quad (2)$$

Using the energy shift in Eq. 1 the values of average size of the CdS nanoparticles have been estimated as 1.45 nm and 1.40 nm in radius in the Y- and Z-type LB films, respectively.

3.2 Atomic force microscopy (AFM) results

Figure 5 shows the change in surface morphology for 15 and 10 layer Y- and Z-type LB films before and after H_2S gas exposure, respectively. LB films yield significant morphological changes after H_2S gas exposure. The LB films roughness increased because of CdS nanoparticles formation in the LB films layers. In addition, Z-type film roughness is more than Y-type film roughness.

3.3 Electrical measurement results

Effect of the CdS nanoparticles on electrical properties of the LB samples is also investigated by measuring room temperature I–V characteristics. Figures 6 and 7 show I–V curves for Y- and Z-type LB films before and after H_2S gas exposure, respectively. The I–V curves show exponential behaviour regardless of film thickness. However, in Y-type films there is an increase in the current value as opposed to the Z-type films where current decreases upon formation of CdS nanoparticles. Type of the LB film significantly influences the conductivity upon nanoparticle formation. The aggregation of CdS nanoparticles in Z-type IBI LB film layers decrease the conductivity value, which is believed to be caused by the increase in the film thickness due to formation of CdS nanoparticles [5, 21]. The conductivity for the Y-type IBI film contains CdS nanoparticles increased. CdS nanoparticles were formed within the Y-type LB film between the head of molecules. The formed of semiconducting CdS nanoparticles in the Y-type insulating LB films must affect the film conductivity. The increase in conductivity is naturally expected [22]. We considered that these conductivity increments were occurred by the semiconducting CdS nanoparticles than increase in the film thickness. But, we couldn't answer an exact solution. Current values for CdS nanoparticles have formed

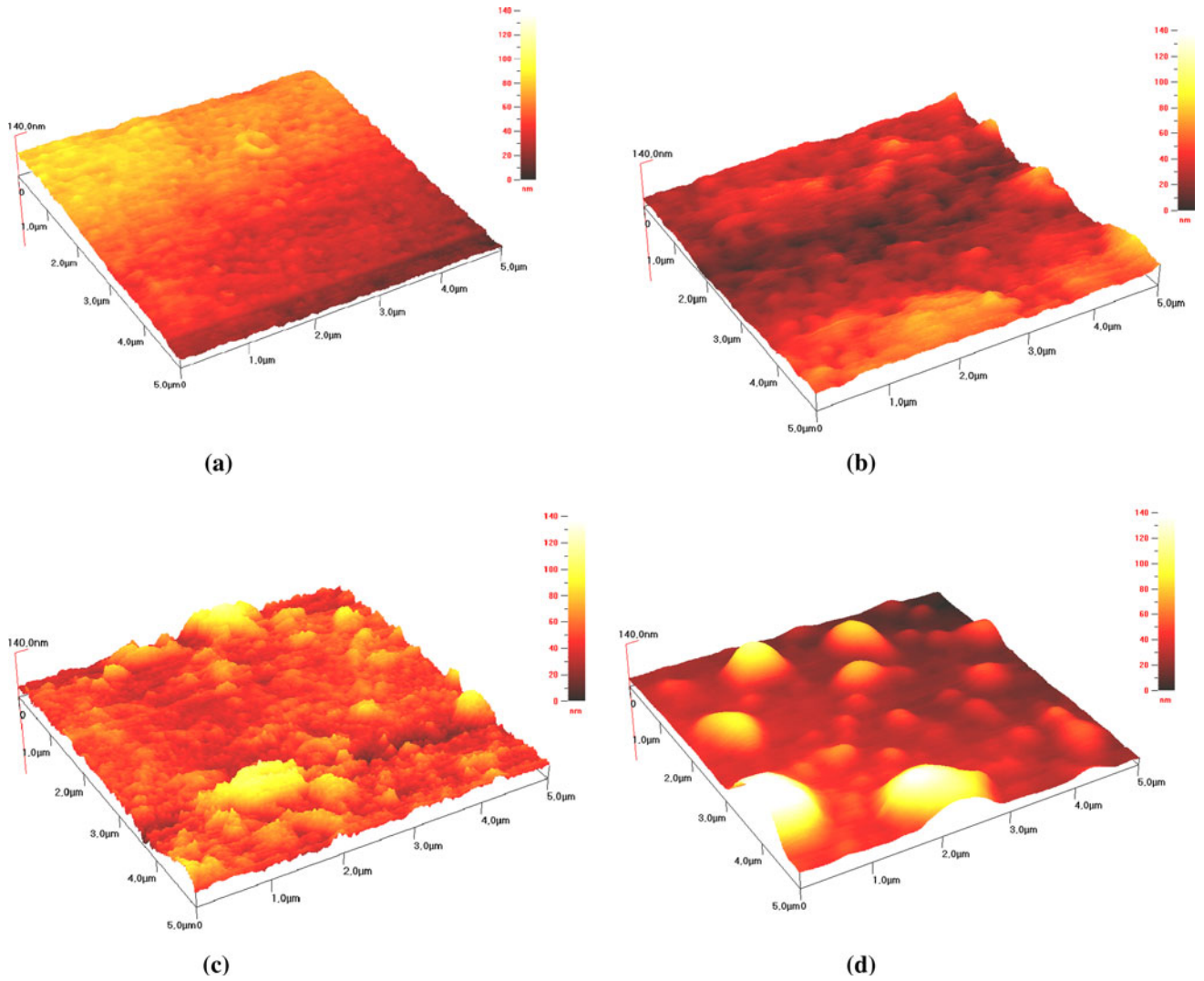

Fig. 5 AFM images for **a** Y-types 15 multilayers before H_2S gas exposed, **b** Y-types 15 multilayers after H_2S gas exposed, **c** Z-types 10 multilayers before H_2S gas exposed, **d** Z-types 10 multilayers after H_2S gas exposed

in IBI LB film layers are higher than for Cd^{2+} doped IBI LB film layers [10].

All LB films in the voltage range indicate the exponentially increasing current. In order to explain conduction process through LB films and the effect of the CdS nanoparticles on conductivity, ln J versus $V^{1/2}$ are plotted in Figs. 8 and 9. The relation between ln J and $V^{1/2}$ shows rather linear dependence which suggests that conduction is governed by either Poole–Frankel or Schottky mechanism.

The conduction through the LB films under investigation can be explained by Schottky conduction mechanism, which is given by [23]:

$$I = \overset{*}{A} \cdot A \cdot T^2 \exp\left(\frac{-e\varphi}{kT} + \beta V^{1/2}\right) \tag{3}$$

where e is the electronic charge, A is the metal contact area, T is absolute temperature, k is the Boltzmann's constant, φ is the potential barrier, $\overset{*}{A}$ is the Richardson constant, V is the applied voltage, and β is the Poole–Frankel field-lowering coefficients given by:

$$\beta = \frac{e}{kT}\left(\frac{e}{\pi\varepsilon_o\varepsilon_r d}\right)^{1/2} \tag{4}$$

Here ε_r is the dielectric constant of the films, ε_0 is the permittivity of free space, d is the film thickness.

The intercept of the linear curve with the ln J axis at $V = 0$ can be expressed in terms of barrier height (φ) and temperature using Eq. 3:

$$\ln J = \ln\left(\overset{*}{A}T^2\right) - \left(\frac{e}{kT}\right)\varphi \tag{5}$$

Using the value of Richardson constant for free electron and using the intercept values in Figs. 8 and 9, the barrier heights were calculated and given in Tables 1 and 2.

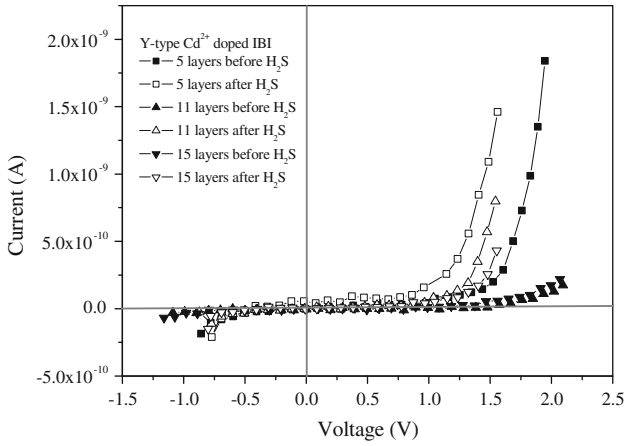

Fig. 6 Room temperature I–V *graph* of the films before (*filled square*, *filled triangle*, *filled circle*) and after (*open square*, *open triangle*, *open circle*) exposing H_2S gas for Y-type Cd^{2+} doped IBI

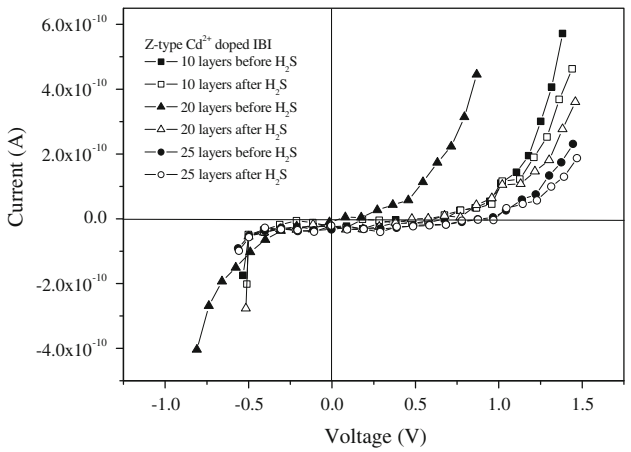

Fig. 7 Room temperature I–V *graph* of the films before (*filled square*, *filled triangle*, *filled circle*) and after (*open square*, *open triangle*, *open circle*) exposing H_2S gas for Z-type Cd^{2+} doped IBI

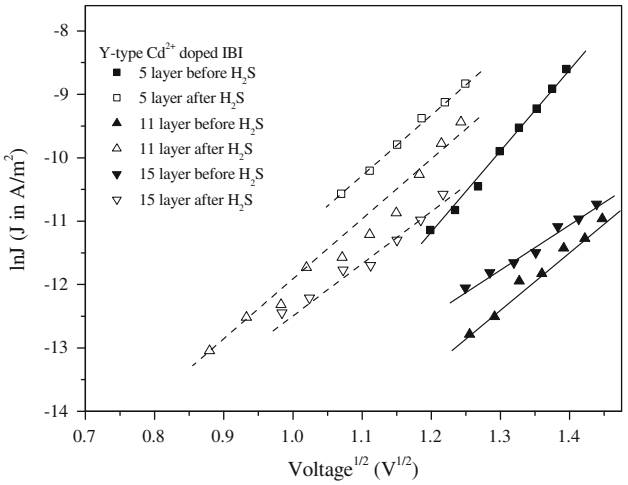

Fig. 8 *Plot* of ln *J* versus $V^{1/2}$ for different layers before (*filled square*, *filled triangle*, *filled circle*) and after (*open square*, *open triangle*, *open circle*) H_2S exposure for Y-type Cd^{2+} doped IBI

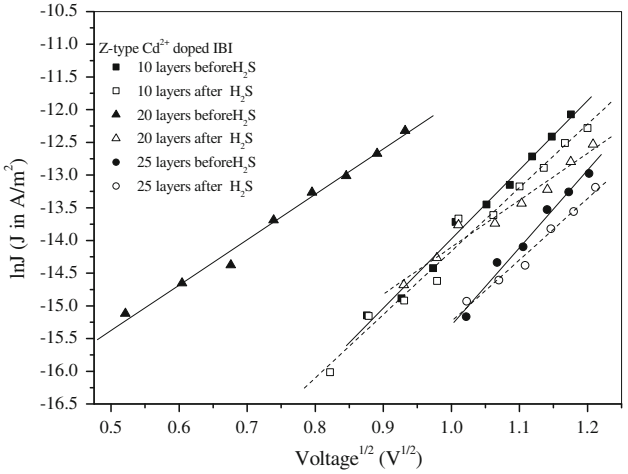

Fig. 9 *Plot* of ln *J* versus $V^{1/2}$ for different layers before (*filled square*, *filled triangle*, *filled circle*) and after (*open square*, *open triangle*, *open circle*) H_2S exposure for Z-type Cd^{2+} doped IBI

In literature, the barrier height of 22-tricosenoic acid LB film is calculated by using a similar approach [24].

Average barrier height for exposed samples is calculated to be 1.17 eV for Y-type films and shown in Tables 1 and 2. Average barrier height of Y-type LB film is slightly less than average barrier height of Z-type. Upon H_2S gas exposure all LB Y- and Z-type samples have shown a consistent decrease in barrier height except for Z-type 20 layers LB film [10]. The change in barrier height after H_2S exposure can be attributed to the partially destroyed layer-by-layer film order caused by the formation of CdS nanoparticles within the monolayers [5].

From the Tables 1 and 2, after H_2S exposure, barrier potential value for the LB film with CdS nanoparticles is slightly higher Z-type LB film than that of the Y-type LB film. This difference in the barrier potential barrier values could be due to variation of the size of nanoparticles in Y- and Z-type LB film layers.

Table 1 Calculation details for barrier height energy of Y-type Cd^{2+} doped IBI films

Number of layers	H_2S treatment	Intercept of ln *J* axis	Barrier height φ (eV)
5	Before	−26.97	1.32
	After	−21.02	1.17
11	Before	−24.60	1.26
	After	−21.53	1.18
15	Before	−20.54	1.16
	After	−20.06	1.15

Table 2 Calculation details for barrier height energy of Z-type Cd^{2+} doped IBI films

Number of layers	H_2S treatment	Intercept of ln J axis	Barrier height φ (eV)
10	Before	−24.81	1.27
	After	−23.55	1.24
20	Before	−19.07	1.12
	After	−22.97	1.22
25	Before	−27.07	1.32
	After	−25.19	1.28

4 Conclusions

Wide band gap CdS semiconducting nanoparticles were formed within the organic film 1,3-bis-(*p*-iminobenzoic acid)indane (IBI) after exposing the multilayered films containing Cd^{2+} ions to H_2S gas. A blue-shift relative to bulk CdS in UV–Vis absorption spectra in both Y- and Z-type LB films is observed. AFM images show that the formation of the CdS nanoparticles in the LB film layer increase Z-type film roughness than Y-type film roughness. It was observed that formation of the nanoparticles causes an increase in current in the Y-type and a decreased in current in the Z-type LB films. These results were attributed to the existence of the nanoparticles causing disordering in layer-by-layer structure of the multilayered films. Small CdS nanoclusters were formed within LB film after exposure of H_2S gas. The size of the clusters was obtained as 1.45 and 1.40 nm for Y- and Z-type films, respectively. By assuming Schottky conduction mechanism the average barrier height was found to be as 1.25 and 1.17 eV for unexposed samples and 1.18 and 1.25 eV value upon formation of the CdS nanoparticles, respectively in the Y- and Z-type films.

Acknowledgments Financial support from Ankara University Research Office (BAP) (Project code: AU-BAP 2003-07-45-016) is gratefully acknowledged. The authors also would like to thank S. Uzun, S. Durkut and M. Evyapan for their help.

References

1. R.W. Samokhvalov, M. Gurney, S. Lahav, H. Cohen, R. Cohen, J. Naaman, Phys. Chem. B **107**, 4245–4252 (2003)
2. P. Mandal, R.S. Srinivasa, S.S. Talwar, S.S. Major, Appl. Surf. Sci. **254**, 5028–5033 (2008)
3. H. Sari, T. Uzunoglu, R. Capan, N. Serin, T. Serin, C. Tarimci, A.K. Hassan, H. Namli, O. Turhan, J. Nanosci. Nanotechnol. **7**, 2654 (2007)
4. C. Tiseanu, R.K. Mehra, R. Kho, M. Kumke, J. Phys. Chem. B **107**, 12153–12160 (2003)
5. A.V. Nabok, B. Iwantono, A.K. Hassan, A.K. Ray, T. Wilkop, Mater. Sci. Eng. C **22**, 355–358 (2002)
6. J. Ma, G. Tai, W. Guo, Ultrason. Sonochem. **17**, 534–540 (2010)
7. D.Y. Protasov, W.B. Jian, K.A. Svit, T.A. Duda, S.A. Teys, A.S. Kozhuhov, L.L. Sveshnikova, K.S. Zhuravlev, J. Phys. Chem. C **115**, 20148–20152 (2011)
8. A. Nabok, A.K. Ray, S. Iwantono, A. Hassan, M. Simmonds, IEEE Trans. Nanotechnol. **2**(1), 44–49 (2003)
9. D.Y. Godovsky, Device applications of polymer–nanocomposites. Adv. Polym. Sci. **53**, 163–205 (2000)
10. R. Capan, A.K. Ray, A.K. Hassan, Thin Solid Films **515**, 3956–3961 (2007)
11. E.S. Smotkin, C. Lee, A.J. Bard, M.A. Campton, T.E. Mallok, S.E. Webber, J.M. White, Chem. Phys. Lett. **152**, 265–268 (1998)
12. A.V. Nabok, T. Richardson, F. Davis, C.J.M. Stirling, Langmuir **13**, 3198–3201 (1997)
13. S.B. Jung, C. Kim, Y.S. Kwon, Thin Solid Films **438–439**, 27–32 (2003)
14. P.A. Antunes, C.M. Santana, R.F. Aroca, O.N. Oliveira Jr., C.J.L. Constantino, A. Riul Jr., Synth. Met. **148**, 21–24 (2005)
15. T. Uzunoglu, R. Capan, H. Sari, Mater. Chem. Phys. **117**, 281–283 (2009)
16. T. Uzunoglu, H. Sari, R. Çapan, H. Namli, O. Turhan, J. Optoelectron. Adv. Mater. **11–4**, 515–519 (2009)
17. M. Parhizkar, N.P. Kumar, B. Shukla, R.S. Srinivasa, S. Vitta, K. Nigvendra, S.S. Talwar, S.S. Major, Colloids Surf. A Physicochem. Eng. Aspects **177**, 257–258 (2005)
18. V. Erokhin, S. Carrara, H. Amenitch, S. Bernstoff, C. Nicolini, Nanotechnology **9**, 158–161 (1988)
19. L.E. Brus, J. Chem. Phys. **80**, 4403 (1984)
20. A.V. Nabok, T. Richardson, C. McCartney, N. Cowlam, F. Davis, C.J.M. Stirling, A.K. Ray, V. Gacem, A. Gibaud, Thin Solid Films **327–329**, 510–514 (1998)
21. Suryajaya, A.V. Nabok, A. Tsargorodskaya, K. Hassan, F. Davis, Thin Solid Films **516**, 8917–8925 (2008)
22. A. Nabok, *Organic and Inorganic Nanostructures* (Artech House, Norwood, 2005), p. 150
23. S.M. Sze, *Physics of Semiconductor Devices* (Wiley, New York, 1981), p. 250
24. N.J. Geddes, J.R. Sambles, W.G. Parker, N.R. Couch, D.J. Jarvis, J. Phys. D Appl. Phys. **23**, 95–102 (1990)